Particle Flow and Heat Transfer in Fluidized Bed-in-Tube Solar Receivers

Alex Le Gal[1], Benjamin Grange[1], Ronny Gueguen, Michael Donovan, Jean-Yves Peroy, Gilles Flamant[2, a)]

[1] PhD, research engineer, Processes, materials and solar energy laboratory, PROMES-CNRS (UPR 8521), 7 rue du four solaire, 66120 Font-Romeu Odeillo, France
[2] corresponding author, PhD, Professor, Processes, materials and solar energy laboratory, PROMES-CNRS (UPR 8521), 7 rue du four solaire, 66120 Font-Romeu Odeillo, France
[a)] Corresponding author: Gilles.Flamant@promes.cnrs.fr

Abstract. This work is part of the European project "Next-CSP" which aims to develop a next generation of concentrated solar power plants using the particle technology and, particularly, the fluidized particle-in-tube technology working at high temperature (>700°C). A 3MWth pilot unit including a solar receiver, storage tanks, a heat exchanger and a gas turbine is under assembly at the top of a solar tower (Themis-France) to demonstrate this technology. The unit will use the fluidized particle-in-tube solar receiver concept. The scaling up of this concept needs researches on the gas-particle flow structure evolution along the tube and on wall-to-fluidized particles heat transfer. Therefore, several experimental set-ups were implemented to study the particle flow and heat exchanges in order to define the best operational conditions for the full-scale 3MW test unit. The first one is a cold experiment with three 3m-long transparent tubes implemented to study the stability of dense particle suspension (DPS) flow in tube and the flow distribution between the different tubes. 3m is the length of the solar receiver tubes. The second one is an on-sun experiment equipped with a one meter-long finned tube to collect data on the distribution of wall surface and particles temperature, thermal exchange and thermal performance useful for further modelling and up scaling. Experiments with the cold mockup indicate that stable particle flowrate ranging from 10 to 340 kg/m^2.s (0.015 to 0.53 g/s) can be obtained per tube with mean particle volume fraction in the range 0.29-0.36. Solar experiments with finned tube designed to increase the heat exchange between the particle suspension and the irradiated tube result in rather constant values of the heat transfer coefficient at about 1200 ± 400 W/m².K for particle mass flux between 40 and 110 kg/m^2.s.

1. INTRODUCTION

The European project Next-CSP **[1]** gathers ten partners with the aim at developing a next generation of concentrated solar power plants using higher temperatures and integrating a direct energy storage. Among the three main options of particle receiver **[2]**, namely the falling curtain, the centrifugal receiver and the fluidized bed, the Next-CSP technology belongs to the latter. It is based on upward flowing dense particle suspension used as heat transfer fluid **[3]**. It consists in a tubular solar receiver in which the heat transfer fluid is upward flowing fluidized particles, a hot storage tank, a fluidized bed heat exchanger and a cold storage tank. The main advantages of this technology are:

- The possibility to reach higher temperature than conventional heat transfer fluids (steam, oil, molten salts) [**4],[5]**. Temperatures up to 750°C are targeted which could considerably improve the thermodynamic cycle efficiency,
- The direct storage of heat through the heat transfer fluid,
- No freezing problems compared to molten salts,
- The control of dust formation using a closed loop of particles including a filtering unit,
- The scalability of the concept (multi-tubular solar receiver),

- Low gas velocity (very small particle attrition) and large solid fraction (about 30% and more) compared to circulating fluidized bed (less than 10%).

The main drawback is the limited heat exchange between particles and the receiver wall surface that have a direct influence on the receiver surface temperature. Indeed the surface temperature of the receiver is limited by material mechanical properties. Therefore, the improvement of heat transfer is crucial justifying the implementation of lab-scale experiments for measuring the heat exchange coefficient between the receiver tubes and the upward flow of fluidized particles. Another open question was the capacity of the system to operate at high particle flow rates, typically larger than 0.1 g/s per tube (about 60 kg/m^2.s with respect to the tube section) and the stability of the particle flow along the tube height. A cold mock-up was constructed to examine these issues.
A previous work **[6]** involving a 0.5m long solar-heated tube highlighted the influence of the particle volume fraction of the suspension and the particle mean velocity on heat transfer. The higher the particle velocity, the higher the heat transfer coefficient because of particle mixing increases and the higher the particle volume fraction the higher the heat transfer coefficient due to the improved contact area with the tube. This first study has been performed with silicon carbide particles. The particle flowrate varied from 7.4 to 24.6 kg/m².s, this flow rate was then extended to 45 kg/m².s and 750°C particle temperature **[7].** The Next-CSP 3MWth pilot plant will use different conditions such as 3 meters long tubes and higher particle flowrates (about 75 kg/m².s at nominal condition). Moreover, olivine particles were selected as heat transfer medium instead of silicon carbide **[8]**. These parameters were defined from modeling and previous experimental campaigns **[9],[10],[11]**. Results on similar conditions are missing therefore two experimental mock-up were implemented to study particle suspension density, flowrate, flow stability and try to correlate these parameters with heat transfer.

2. EXPERIMENTAL SETUP

Two experimental setups were developed to gain a better understanding of the link between particle suspension characteristics and heat transfer. A cold experiment was designed to characterize the dense suspension (mean and local suspension density -or particle volume fraction- and fluidization regimes) as a function of air velocity (main and aeration), height along the tube and particle mass flowrate. The second one is an on-sun experiment developed to measure heat transfer coefficient as a function of previous parameters.

2.1 Particles

Olivine particles have been chosen to serve as heat transfer fluid and heat storage medium. These particles have been selected because they have attractive thermophysical properties (density, thermal conductivity, specific heat capacity) and a high thermal resistance without risks of sintering or attrition at operating temperatures. These particles also present acceptable health and safety hazards with a negligible environmental impact [**8]**. Characteristics of the particles are listed in Table 1.

Table 1. Main characteristics of the particles used during the experiments

Particle	Composition	Mean diameter (d_{50}) - µm	Sauter diameter (d_{32}) - µm	Density - kg/m^3	Bulk conductivity at 800°C – W/mK
Olivine	MgO 49.5%, SiO_2 42%, Fe_2O_3 7.5%	59 *	30	3300	0.56

*After elimination of fines (< 20 µm)

The heat capacity of olivine used for thermal calculations is calculated from the following polynomial formula:

$$C_p = 9.70 * 10^{-8}T^3 - 2.62 * 10^{-4}T^2 + 0.73T + 8.06 * 10^2 \quad \text{J/kg.°C}$$

With T the temperature in °C. The range of validity of the previous polynomial is 400°C-1200°C **[8]**. For temperature lower than 400°C the heat capacity of olivine is fixed at 1 kJ/kg.°C.

2.2 Cold Experiment

To study the particle flow behaviour, cold experiments (without solar heating) were performed with a dedicated setup (Fig. 1). Three vertical transparent tubes (3-meters long) are plunged into a fluidized bed dispenser and are connected to storage tanks at the outlet. During the first set of experiments, a single tube only was used. The gas injection in the dispenser uniformly distributes the fluidization air through a porous distribution plate. A second air injection (Aeration) is placed at the tubes bottom, just above the dispenser top, to increase the airflow rate inside the tubes and stabilize the particle flow **[12].** Particles (olivine) are firstly fluidized in the dispenser and the dense particles suspension upward flowing is then govern by a pressure control valve in the dispenser. By closing this valve, the pressure in the freeboard of the dispenser increases and the fluidized particles flow up through the tubes. The mock-up was equipped with differential pressure gauges (*Rosemount 2051 pressure transmitter*) along the tubes to measure the differential pressure drops at different heights and the pressure fluctuation with time. A weighting scale was implemented to measure the particle flowrate.

The influence of the particle flowrate as well as the secondary air injection on fluidization behaviour of the upward bubbling dense suspension was studied.

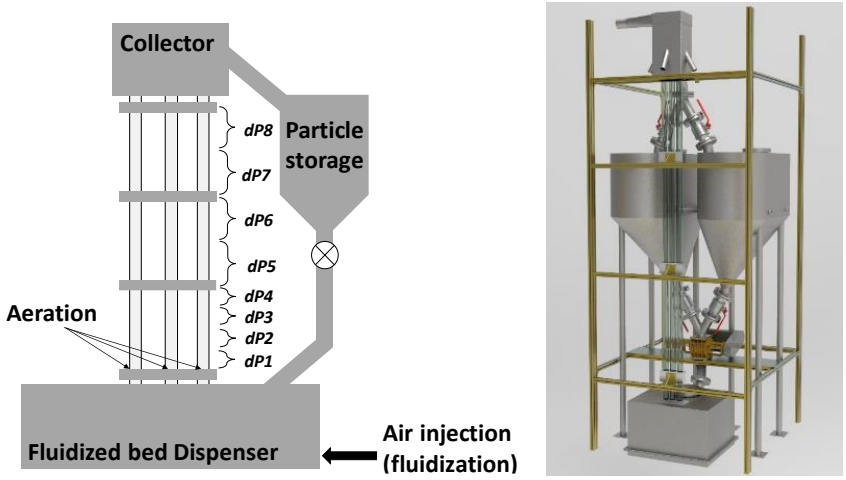

(a) (b)

Figure 1. Schematic description of the cold experimental setup (a), and 3D view (b)

2.3 On-Sun Experiment

2.3.1 Tubular Solar Receiver Description

The lab-scale solar experimental setup is shown in Figures 2a and 2b (3D view). The particles were fed to the dispenser fluidized bed (1) from a cold storage tank (7), through a rotary valve (6) that controlled the particle mass flow rate. The particles were fluidized in the dispenser, then under the effect of pressure, the fluidized particles flew upward in the 1m-long absorber tube (3) (Inconel 601, 50 mm OD, 2 mm wall thickness). The length of the tube was limited to 1m because of the available solar facility. The tube was manufactured with fins welded at the wall along the tube axis. A secondary airflow (Aeration) was injected at the bottom of the absorber tube to stabilize the suspension flow and to create bubbles that mix the particles and thus improve the heat transfer. The tube was located in 1m-long refractory cavity (4 & fig.2.a) irradiated by the concentrated solar flux. At the tube outlet, the particles reached the collector fluidized bed (5) and then descended through an exit tube (8) to a scale (9) that continuously measured the outlet mass. Electric heaters (2) were inserted in the dispenser for preheating the particles (if necessary). The experimental setup was designed for batch operations. A dust collector have been implemented, it consists of a baghouse filter connected to the top of the collector fluidized bed that recovers the particles entrained in the fluidization gas. A very small amount of particles was collected during the experimental campaign.

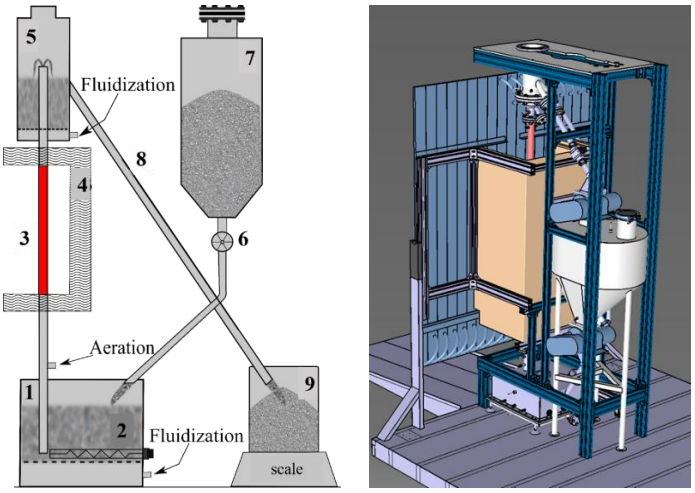

(a) (b)

Figure 2.a: Schematic cross-sectional view of the vertical reactor final batch setup (1.Dispenser fluidized bed, 2.Electrical heaters, 3.Solar absorber metallic tube, 4.Solar receiver cavity, 5.Collector fluidized bed, 6.Rotary valve feeder, 7.Solid storage tank, 8.Outlet tube 9.Container on weighing scale); 2b: 3D representation of the complete set up mounted at the focus of the solar furnace

The external surface of the tube was painted with absorbing black paint (Pyromark® 2500). The tube was set in a monolithic refractory cavity with a 0.1 x 1m aperture that could stand temperature up to 1350-1400°C, and which was embedded in a 0.75 x 0.6 x 1.45 m receiver filled with insulating boards (Insulfrax® 110L by UNIFRAX, suitable up to 1200°C).

2.3.2 Temperature and Pressure Sensors

The overall experimental setup was equipped with 49 K-type thermocouples, 9 pressure gauges and a scale to measure the particle mass flow rate.

The thermocouples used for measuring particles temperature have an uncertainty of ±1.5K, therefore the temperature difference between the inlet and the outlet of the tube ΔT_p is given with an uncertainty of ±3K.

A data acquisition system has been developed to record all these temperatures and pressures. The user interface allowed a direct reading of all parameters during experimental campaigns and data were recorded in a file for further analysis. The main critical parameters are the tube temperature profile, the differential pressure in the dispenser (indicating the mass of particles remaining in the vessel), the total pressure in the freeboard of the dispenser (the driving pressure) and the particle temperature difference between the inlet (dispenser) and the outlet (top of the irradiated zone). The particle mass flow rate was measured using a scale with a direct reading and recorded on another computer. The instantaneous variations were recorded as well as the 5 seconds, 30 seconds, 1-minute and 2 minutes sliding averages to check the stabilization of the particle mass flow rate.

3. RESULTS

3.1 Particle Flow in Tube (cold experiments)

3.1.1 Minimum fluidization velocity

The differential pressure drop (height between the probes: 20 cm) as a function of the air velocity was measured in a 9 cm ID tube to determine the minimum fluidization velocity (U_{mf}) of the particles. Figure 3 shows the pressure drop as a function of the air velocity. Three measurements were realized and the measured U_{mf} is 0.400 ± 0.048 cm/s. In the following experiment, the fluidization air velocity in the dispenser was set at 0.973 ±0.004 cm/s, which corresponds to 2.4 U_{mf}.

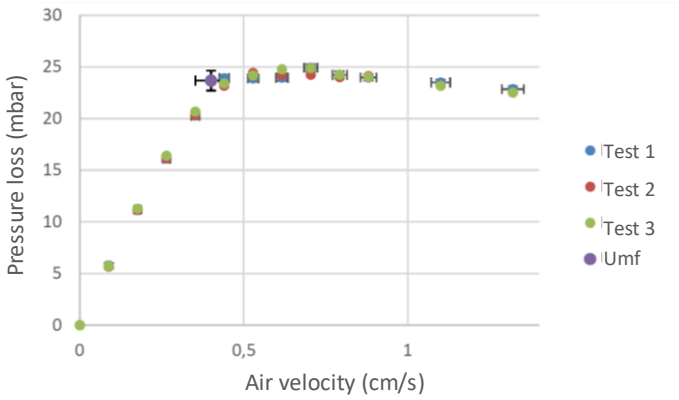

Figure 3. Determination of the olivine particles minimum fluidization velocity (U_{mf}).

3.1.2 Mean particle volume fraction with respect to particle mass flowrate

More than forty experiments have been conducted to study the evolution of the particle volume fraction in the tube as a function of the particle mass flowrate and the air velocity. The pressure drop through the tube is considered equal to the hydrostatic pressure of the suspension. It means that pressure losses due to friction at the wall are neglected. The mean particle volume fraction is calculated from pressure drop measurements using the following formula:

$$\Delta P = \left(\alpha_p . \rho_p + \varepsilon . \rho_g\right) . g . \left(h_{top} - h_{bottom}\right) \quad (1)$$

With, ΔP: the pressure drop
α_p: the particle volume fraction
ρ_p: the particle density
ε: the suspension voidage (α_p=1- ε)
ρ_g: the gas density
g: the gravitational acceleration
$(h_{top} - h_{bottom})$: the distance between the pressure sensors

By neglecting the air density in front of the particle density the particle volume fraction is expressed as followed:

$$\alpha_p = 1 - \varepsilon = \frac{\Delta P}{\rho_p . g . (h_{top} - h_{bottom})} \quad (2)$$

Figure 4 presents the averaged particle volume fraction over the tube height (α_h) as a function of the particle flowrate for several aeration air flowrate. The mean particle volume fraction ranges between 0.29 and 0.36 and is not dependent on the particle flowrate. Nevertheless, the aeration airflow rate affects the suspension density, the higher the airflow the lower the density. By varying the aeration from 500 g/h to 1400 g/h, the particle volume fraction decreases from 0.36 to 0.29.

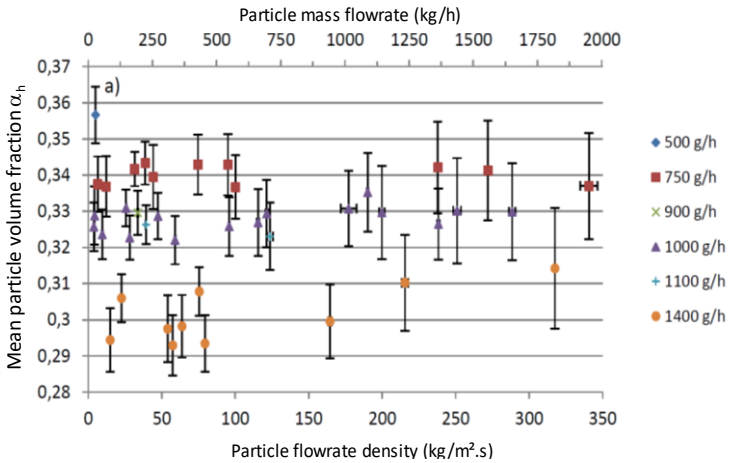

Figure 4. Particle volume fraction averaged over the tube height as a function of particle flowrate with aeration mass flowrate as parameter (right column).

3.1.3 Mean particle volume fraction with respect to air velocity

Then the influence of the air velocity (air from fluidization + aeration) on particle volume fraction was studied. Since the particle flowrate does not influence the particle volume fraction (cf. 3.1.2), experiments were realized with different particle flowrates. Figure 5 shows the averaged particle volume fraction over the tube height (α_h) as a function of the air velocity. A clear correlation between these two parameters is highlighted. By increasing the air velocity from $23xU_{mf}$ to $65xU_{mf}$ the particle volume fraction averaged over the tube height decreases from 0.35 to 0.30 respectively. Given that the fluidization air in the dispenser is constant, this figure shows the influence of the aeration and follows the same trend as fig. 4.

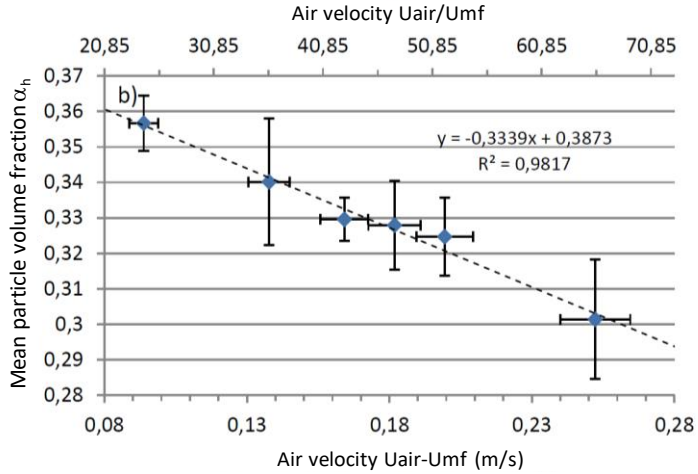

Figure 5. Particle volume fraction averaged over the tube height as a function of the air velocity

3.1.4 Particle volume fraction over the tube height

The particle volume fraction was plotted as a function of the tube height for several particle flowrates and air velocities to emphasize the variations of volume fraction along the tube height. Figure 6 presents the evolution of the particle volume fraction as a function of the tube height for several particle mass flowrate and aeration air flowrate.
For a particle flowrate Gp=12 kg/m².s and an aeration airflow of 750 g/h (fig. 6.a), the particle volume fraction increases with the tube height from 0.33 to 0.35. For a same aeration airflow and a particle flowrate Gp=39 kg/m².s (fig. 6.b), the volume fraction is stable along the tube at 0.34. Finally, for Gp=251kg/m².s and an aeration airflow of 1000 g/h (fig. 6.c) the slope becomes negative and the particle volume fraction decreases along the tube from 0.35 to 0.31.

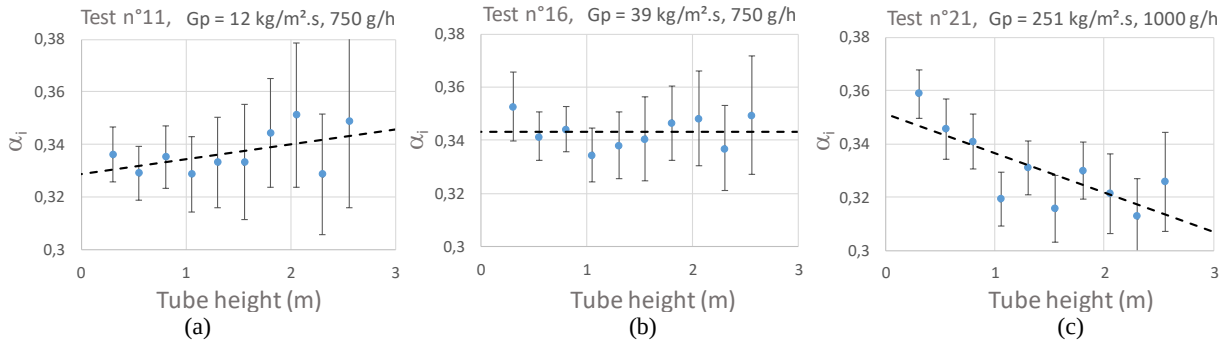

(a) (b) (c)

Figure 6. Examples of particle volume fraction evolution as a function of the tube height for several particle flowrate and air flowrate.

It was observed that the volume fraction is not constant along the tube. A linear evolution was measured and the volume fraction can be expressed as followed:

$$\alpha_i = x\bar{h} + y \qquad (3)$$

With, α_i the particle volume fraction at the height i
$\bar{h}$ the height in tube above the aeration
x the slope of the regression line
y the intercept of the regression line

The general trend observed from these experiments is that the aeration does not influence the particle volume fraction distribution along the tube. On the contrary, the particle flowrate has a direct influence on this distribution. By increasing the particle flowrate the slope of the distribution (x) decreases and becomes negative for high particle flowrate. It means that the particle volume fraction became lower at the top of the tube than at the bottom for large particle mass flowrate.

To conclude this study on particle flow in tube it can be said that for a given aeration air flowrate, the increase of the particle mass flowrate leads to a variation of the volume fraction distribution along the tube. However, the averaged density along the total height of the tube remains constant whatever the particle mass flowrate. Therefore, the particle mass flowrate affects only the density distribution along the tube.
On the contrary, the aeration air flowrate have an influence on the averaged density but no influence on density distribution along the tube. The higher the aeration the lower the averaged density. This trend is coherent with previous results obtained at high temperature and short tubes **[6]** and values of the particle volume fraction are comparable to the one measured during previous experiments done at high temperature (from 0.26 to 0.34). The only difference between cold and hot experiments is the slope of the particle volume fraction as a function of the aeration flowrate, at high temperature the volume fraction decrease more rapidly than at ambient because of air thermal expansion. The comparison with the previous work also highlights that the length of the tube does not influence significantly the mean particle volume fraction. The particle suspension has a similar porosity for a 0.5 m and a 3 m-long tube.
Another important conclusion is that the system enables to manage high particle mass flowrate. No limitations were observed up to 350 kg/m².s (0.55 g/s). Moreover, no significant variation of α_p was measured for particle flowrate from 100 to 350 kg/m².s (= 570 to 2000 kg/h) it is still in the range 0.30-0.35.
The next step is to correlate the particle flow in tube with heat exchanges between particles and the tube under concentrated solar flux.

3.2 Heat Transfer (On-sun experiments)

More than 60 on-sun experiments have been done under several solar flux density to evaluate heat transfer as a function of the particle mass flowrate and the aeration air flowrate. The on-sun experiments were carried out in a more restrictive range of particle mass flowrate (25-108 kg/m².s) than cold experiments because thermal equilibrium can not be reached at high particle mass flow rate during batch runs. The power extracted by particles is calculated using the following formula:

$$\Phi_{DPS} = F_p . Cp_p . (T_{p,o,center} - T_{p,i,DiFB}) \quad (4)$$

With:

F_p: the particles mass flow rate in kg/s

Cp_p: the heat capacity of olivine at the mean temperature

$T_{p,o,center}$: the particle temperature at the tube outlet

$T_{p,i,DiFB}$: the particle temperature in the dispenser fluidized bed

Figure 7 plots the power absorbed by the particles (net or useful power) as a function of the particle mass flow rate for different solar power input. The three configurations used (low, medium, high flux) correspond to mean solar flux densities of 236, 368 and 485 kW/m² respectively scaled to a 1000 W/m² DNI. To compare the different experiments done at various DNI (in the range 900-1020 W/m²), all the values were scaled to correspond to a direct normal irradiation of 1000 W/m². The low solar flux density leads to an extracted power from 11.9 kW to 17.8 kW for respective particle mass flow rates of 25 kg/m².s to 108 kg/m².s. A significant increase of the power transferred to the particle flow is observed for low particle mass flow rates from 25 to 40 kg/m².s and then the increase of power is smoother as a function of the mass flow rate. For the medium solar flux configuration, the power extracted varies from 23.2 kW to 28.7 kW for particles mass flow rates of 38 and 98 kg/m².s respectively. With the highest solar flux input, the range of the power absorbed by the particles varies from 26 to 32 kW for respective particles mass flow rate of 35 and 95 kg/m².s.

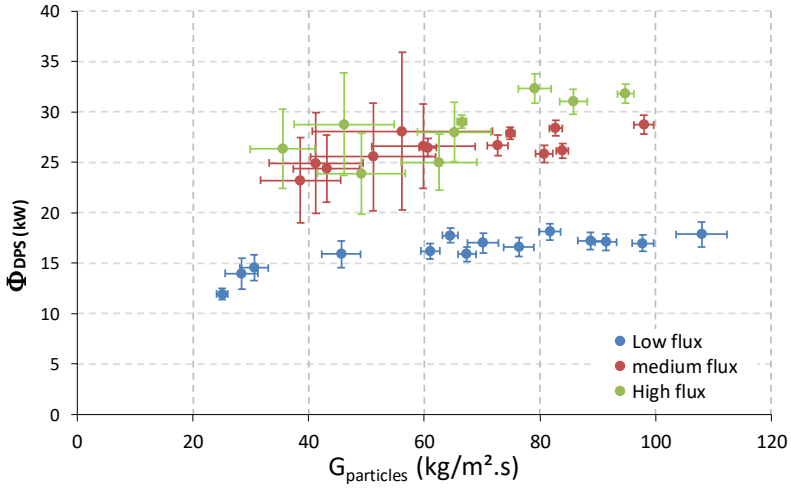

Figure 7. Power extracted by particles as a function of the particle mass flow rate and solar power input. Φ_{DPS} are scaled at a DNI of 1000 W/m².

A global wall-to-fluidized particle heat transfer coefficient, **h_{tube},** was calculated over the tube height exposed to concentrated solar radiation as followed:

$$h_{tube} = \Phi_{DPS}/(A . \Delta T_{lm}) \quad (5)$$

With:

Φ_{DPS}: from eq.4

A: the internal surface area of the irradiated part of the receiver tube

ΔT_{lm}: the logarithmic mean temperature difference

and,

$$\Delta T_{lm} = \frac{\left(T_{w,i}^{int} - T_{p,i}\right) - \left(T_{w,o}^{int} - T_{p,o}\right)}{\ln \frac{T_{w,i}^{int} - T_{p,i}}{T_{w,o}^{int} - T_{p,o}}} \quad (6)$$

With :

$T_{w,i/o}^{int}$: the internal wall temperature (inlet/outlet)

$T_{p,i}$: the inlet particles temperature

$T_{p,o}$: the outlet particles temperature

Figure 8 presents the variation of the wall-to-fluidized bed heat transfer coefficient as a function of the particle mass flux density for the low solar flux configuration tested during the experimental campaign.

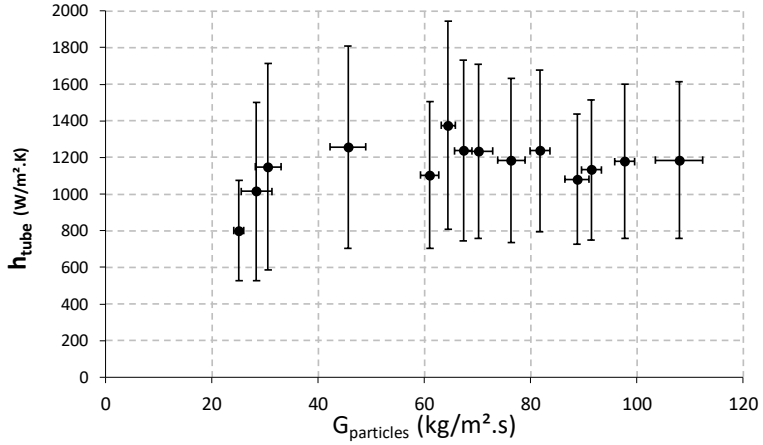

Figure 8. Heat transfer coefficient between the fluidized particles and the finned tube calculated as a function of the particles mass flux density at low solar flux. Inlet particle temperature at ambient, aeration 0.29 Nm^3/h. The reference surface is the internal surface of the bare tube.

The results are very sensitive to the temperature measurements of particles and tube wall (cf. eq.6), consequently, the uncertainty on h_{tube} is large. However, the results are very coherent leading to reduced variations of h_{tube} with particle mass flux density in the range 40-110 kg/m².s in the range 1100-1400 W/m².K. The heat transfer coefficient reaches a plateau at about 1200 ± 400 W/m².K for particle mass flux density between 40 and 110 kg/m².s. For particle mass flux density from 20 to 40 kg/m².s, the heat transfer coefficient increase from 800 to 1200 W/m².K.The aeration airflow rate does not influence significantly the heat transfer coefficient. h_{tube} reaches 1034, 1070 and 1083 W/m².K for secondary air flowrate of 362, 620 and 865 g/h respectively; this variation is in the range of measurement uncertainty. The trend can be analyzed according to two contrary effects. First, the increase of the aeration flowrate results in a better particle mixing that should lead to an increase of the heat transfer coefficient. But, second, the particle suspension is more diluted according to our cold measurements, consequently, the effect on h_{tube} is balanced.

4. CONCLUSION

These two experimental mock-ups result in new findings about the behavior of both particle flow in tube and particle-to-wall heat exchange.

- The system enables to manage high particle mass flowrate. No limitations were observed up to 350 kg/m².s (0.55 g/s) per 46mm ID tube.
- The mean particle volume fraction is dependent of the aeration flowrate, the higher the airflow the lower the averaged density. On the opposite, the particle flowrate do not influence the mean particle volume fraction but only its distribution along the tube height. The higher the particle mass flowrate the lower the particle volume fraction at the top of the tube. These experiments were realized at ambient temperature. In hot conditions (on-sun experiments), the expected effect of air heating up along the tube is a decrease of the particle volume fraction at the top of the tube compared to the bottom due to air thermal expansion. This evolution was predicted by numerical simulation **[11].**
- The global heat exchange coefficient, h_{tube}, presents two different behaviors as a function of the particle mass flowrate. For particle flowrates from 20 to 40 kg/m².s, h_{tube} increases from 800 to 1200 W/m².K. For higher particle flowrates the heat exchange coefficient reaches a plateau at 1200 W/m².K. Consequently, h_{tube} does not vary for particle mass flowrate higher than 40 kg/m².s. The aeration does not show any

influence on heat exchange because the two effects counter balance. The higher the airflow, the higher the particle mixing which favors heat exchange but the higher the airflow, the lower the particle volume fraction that reduces heat exchange.

The relation between particle flow structure in the absorber tube and heat transfer is a complex combined effect of mean and local particle volume fraction, particle mixing and bubbling properties of the upward flowing fluidized particle suspension. The temperature and the temperature gradients affect these interactions. An efficient particle mixing favors the wall to particle heat transfer and is promoted by a vigorous bubbling. Consequently, the evolution of the dynamic behavior of the particle flow along the tube height is a very important parameter. A transition from bubbling to slugging was measured in **[13]** for tube height between 0.5 and 1 m. This transition is not expected because it results in a decrease of heat exchange at the wall. Fortunately, an increase of temperature results in an increase of the transition height above 3 m at 600°C. Considering the key importance of the suspension dynamics, the next step of the study will focus on the measurement of the local pressure fluctuations with time that are correlated to the fluidization regime.

5. ACKNOWLEDGMENTS

This project has received funding from the European Union's Horizon 2020 research and innovation program under the grant agreement No 727762 project acronym Next CSP. The French "Investments for the future" program managed by the National Agency for Research under contracts ANR-10-EQPX-49 (SOCRATE) supported the facility. The Occitanie French region funded the cold mockup.

6. REFERENCE

1. Project website: http://next-csp.eu/
2. Ho C.K. *A review of high-temperature particle receivers for concentrating solar power*. Applied Thermal Engineering 109:958–969, 2016
3. Flamant G., Hemati H., *Dispositif collecteur d'energie solaire (Device for collecting solar energy)*, French patent FR 1058565, 2010, PCT extension WO2012052661, 2012
4. Pitz-Paal R., Amin A., Bettzuge M.O., Eames P., Flamant G., Fabrizzi F., Homes J., Kribus A., Van der Lan H., Lopez C., Garcia Novo F., Papagiannakopoulos, P., Pihl, E., Smith, P., Wagner, H-J., *Concentrating solar power in Europe, the Middle East and North Africa: a review of development issues and potential to 2050*. ASME Journal of Solar Energy Engineering 134:024501, 2012
5. Ho C,K., *Advances in central receivers for concentrating solar applications*, Solar Energy, 152, 38-56, 2017
6. Flamant G., Gauthier D., Benoit H., Sans J-L., Garcia R., Boissiere B., Ansart R., Hemati M., *Dense suspension of solid particles as a new heat transfer fluid for concentrated solar thermal applications: On-sun proof of concept*, Chemical engineering science, 102:567-576, 2013
7. Benoit H., Perez Lopez I., Gauthier D., Sans J-L., Flamant G., *On-sun demonstration of a 750°C heat transfer fluid for concentrating solar systems: Dense particle suspension in tube*, Solar energy, 118:622-633, 2015
8. Kang Q., Flamant G., Dewill R., Baeyens J., Zhang H.L. Deng Y.M., *Particles in a circulation loop for solar energy capture and storage*, Particuology, 43:149-156, 2019
9. Perez Lopez I., Benoit H., Gauthier D., Sans J-L., Guillot E., Mazza G., Flamant G., *On-sun operation of a 150 kWth pilot solar receiver using dense particle suspension as heat transfer fluid*, Solar Energy, 137:463-476, 2016
10. Zhang H., Benoit H., Gauthier D., Degreve J., Baeyens J., Perez Lopez I., Hemati M., Flamant G., *Particle circulation loops in a solar energy capture and storage: Gas-solid flow and heat transfer considerations*, Applied Energy, 161:206-224, 2016
11. Benoit H, Ansart R, Neau H, Garcia Trinanes P, Flamant G, Simonin O., *3D numerical simulation of upflow bubbling fluidized bed in opaque tube under high flux solar heating*, AIChE Journal, 64: 3857- 3867, 2018
12. Boissière B., Ansart R., Gauthier D., Flamant G., Hemati M., *Experimental hydrodynamic study of gas-particle dense suspension upward flow for applications as new heat transfer and storage fluid*, The Canadian Journal of Chemical Engineering 93: 317-330, 2015
13. Kong W., Tan T., Baeyens J., Flamant G., Zhang H., *Bubbling and Slugging of Geldart A Powders in small diameter columns*, Industrial and Engineering Chemistry Research 56(14): 4136-4144, 2017.